Highly Stable Amine Functionalized Iron Oxide Nanoparticles Designed for Magnetic Particle Imaging (MPI)

Hamed Arami and Kannan M. Krishnan

Department of Materials Science and Engineering, University of Washington, Seattle, Washington 98195-2120 USA

Magnetic particle imaging (MPI) is a promising medical imaging technology that uses iron oxide nanoparticles (NPs) as clinically safe tracers. The core and hydrodynamic size of these NPs determine the signal intensity and spatial resolution in MPI, whilst their monodispersity when preserved during the biomedical applications, generates a consistently high quality MPI image. Using an effective process to coat the synthesized NPs with amine terminated PEG molecules, we show by dynamic light scattering (DLS) that they are water-soluble with long-term stability in biological media such as phosphate buffered saline (PBS) and sodium bicarbonate buffers and Dulbecco's modified Eagle medium (DMEM) enriched with 10% fetal bovine serum (FBS). Further, using magnetic particle spectroscopy (MPS), to measure the particle response function (PRF), defined as the derivative of the magnetization of the nanoparticles, we predict the MPI performance of these nanoparticles at a driving field frequency of 25 kHz. The MPS efficacy of the functionalized nanoparticles was also monitored over time, and both signal intensity and resolution remained unchanged even after seven days of incubation. This is attributed to the dominant contribution of the Néel relaxation mechanism of the monodisperse and highly stable nanoparticles, which was preserved through the incubation period.

***Index Terms*—Biomedical engineering, functionalization, iron oxide nanoparticles, magnetic particle imaging (MPI).**

I. Introduction

MAGNETIC particle imaging (MPI) is a developing technique that can potentially provide ultra-high tracer mass sensitivity and spatial resolution for tomographic biomedical imaging [1], [2]. It is a magnetic inductive measurement technique, in which a sufficiently large alternating magnetic field results in a non-linear magnetization response, M(t), from the magnetic tracers [1]. Signal localization for imaging is achieved by scanning a field-free point (FFP) across the imaging volume. In the *x-space* approach to MPI image reconstruction [3], the imaging performance can be simply described by the point spread function (PSF), $\mathrm{h(x)} = \mathrm{dM(G} * \mathrm{x)/dx}$, where G is the scanner field gradient along the direction of motion of the FFP. Aside from G, which is a scanner property, the PSF is determined by the tracer particle response function (PRF), $\mathrm{p(H)} = \mathrm{dM/dH}$. In fact, the PSF is a product of the PRF, dM/dH, and the field gradient, dH/dx. Therefore, for a given imaging system, with a well defined field gradient, the spatial resolution and signal intensity in MPI can be maximized by decreasing the PRF full width at half maximum (FWHM) and increasing its peak height [4], [5]. Alternatively, in the frequency domain approach to MPI image reconstruction, a Fourier transform of the signal, F(dM/dt) at each point in the imaging volume is performed and compared to a predetermined system function [6], [7]. F(dM/dt) is unique to the tracer performance and can be used, alternatively, to evaluate imaging performance.

Magnetite (Fe_3O_4) nanoparticles are biocompatible and nontoxic magnetic contrast agents that have been extensively used for MPI [3], [8]. However, the size, monodispersity and stability of these tracers are extremely critical parameters, determining the sensitivity and spatial resolution of the images in MPI [9]. Detachment of the coating molecules in the presence of strong ionic species in the biological media such as blood and adsorption of the proteins are two challenging phenomena resulting in instability of the NPs and the formation of aggregates [2], [10]. These large size aggregates have shorter blood circulation half-life and rapid clearance through the reticuloendothelial system (RES). Also, they have a larger coercivity, and respond by hysteretic reversal, requiring larger applied magnetic field amplitudes [11]. Therefore, when present in a sample, these aggregates decrease the signal intensity and spatial resolution in MPI [4].

We synthesized highly monodispersed oleic acid coated magnetite nanoparticles in an organic solvent with median core size of about 18 nm. Using a silanization method for ligand exchange and subsequent conjugation of bis-amine polyethylene glycol (NH_2-PEG-NH_2) to the surface of the NPs [12]–[15], these particles were transferred to the aqueous phase. The NPs were individually coated without forming aggregates and remained highly stable in different biological media for more than a week maintaining their spatial resolution and signal intensity. The results of this study pave the way for future use of these NPs in various MPI related biomedical applications.

II. Experimental Procedure

The procedure used for synthesis and PEG coating of the NPs is shown in Table I. Monodisperse iron oxide NPs were prepared, based on a method reported previously [8], [16]. Briefly, iron oleate was synthesized and dissolved in 1-octadecene [17], [18] and then a mixture of iron oleate, oleic acid and 1-octadecene was refluxed at 320 °C for 22h under inert argon atmosphere. The molar ratio of iron oleate to oleic acid was adjusted to 1:18. To purify the as-synthesized NPs, we sonicated them in 40 mL of a 1:1 (v/v) mixture of chloroform and methanol and precipitated them three times with a strong magnet. Purified NPs (~30 mg) were dried in vacuum,

Manuscript received November 01, 2012; revised January 07, 2013; accepted January 27, 2013. Date of current version July 15, 2013. Corresponding author: K. M. Krishnan (e-mail: kannanmk@uw.edu).

Color versions of one or more of the figures in this paper are available online at http://ieeexplore.ieee.org.

Digital Object Identifier 10.1109/TMAG.2013.2245110

TABLE I
PROCEDURE USED FOR SYNTHESIS OF PEG COATED NPS

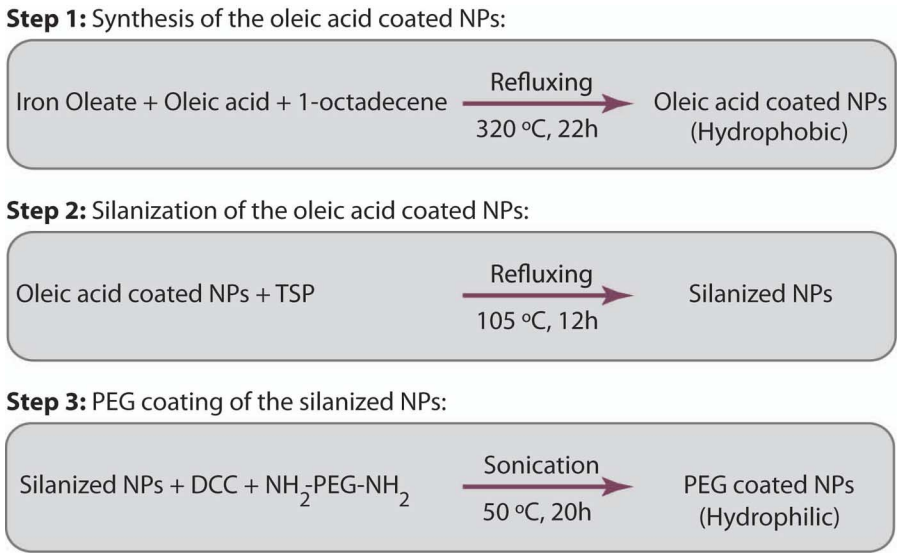

redispersed in 35 mL toluene by 15 min sonication. NPs were functionalized with amine-terminated polyethylene glycol (NH_2-PEG-NH_2), by modification of the procedures described before [13], [15]. First, NPs were silanized by addition of 50 μl of 3-(triethoxysilyl)propyl succinic anhydride (TSP) to the NPs and refluxing the mixture at 105 °C for 12h under argon atmosphere. NPs were then purified by addition of 50 mL hexane and using a strong magnet. Precipitated NPs were dispersed in 7 mL tetrahydrofuran (THF). Dicyclohexylcarbodiimide (DCC, 80 mg) and bis-amine PEG (170mg, MW 2kDa, Laysan Bio Inc.) were added to the NPs and the mixture was sonicated at 50 °C for about 20h. PEG coated NPs were separated by addition of excess hexane and using a strong magnet. Dried NPs were dispersed in 3 mL sodium bicarbonate buffer $(\mathrm{pH} = 8.5)$ and sonicated for 15 min. Size exclusion purification ($\mathrm{Sephacryl_{TM}}$ S-200 gel) was used to remove un-reacted PEG molecules.

We used Inductively Coupled Plasma Atomic Emission Spectrophotometer (ICP-AES, Jarrell Ash 955, US) to determine the iron concentration at each step of the NPs preparation. For long-term stability tests, 50 μL of the NPs were incubated in 1 mL PBS and sodium bicarbonate buffers and DMEM cell culture media enriched with 10% FBS. Dynamic light scattering (Zetasizer Nano, Malvern Instruments, U.K.) was used to monitor the variation of the average hydrodynamic size of the NPs in different media. Transmission Electron Microscope (TEM, FEI TecnaiTM G2 F20, 200 KeV, Hillsboro, OR), equipped with a Gatan CCD camera (Pleasanton, CA) was used for morphological analysis of the NPs before and after the functionalization. For studying the room temperature magnetization (M vs. H) of the NPs, about 100 μL of the liquid samples (100–200 μg of NPs) were transferred to a polycarbonate capsule and analysis were performed using a room temperature vibrating sample magnetometer (VSM, Lakeshore, Weterville, OH). Size of the NPs were calculated using Chantrell method, by fitting the resulted magnetization curves to the Langevin function [19]. We calculated the Brownian relaxation times (τ_B) of the NPs using (1)

$$\tau_B = \frac{3V\eta}{K_B T} \tag{1}$$

Here, V is the hydrodynamic volume of the PEG coated NPs, η is the viscosity of the water at room temperature (10^{-3} N.s/m^2), K_B is the Boltzman's constant (1.38×10^{-23} m^{2}kg.s^{-2}.K^{-1}) and T is the ambient temperature (298 K). Néel relaxation time (τ_N) of the NPs was also calculated using (2)

$$\tau_N = \frac{\tau_0 \sqrt{\pi} \exp(\sigma)}{2\sqrt{\sigma}} \tag{2}$$

in which, τ_0 is $10^{-10}, \sigma = \mathrm{Kv/K_B T}$, v is the volume of core iron oxide and k is the magnetocrystalline anisotropy constant for bulk iron oxide, 11 kJ/m^3 [7].

We used our custom-built MPS, for evaluation of the MPI performance of the NPs [4], [9]. 200 μL of the NPs with known concentration were transferred to microcentrifuge vials that were then inserted into the MPS coils. We repeated each measurement three times using a sinusoidal excitation field of 18.6 mTμ_0^{-1} (peak-peak, $\mathrm{f_0} = 25$ kHz). In this paper, we show the MPS data in the form of PRF (in *x-space*) and the harmonic spectrum (in frequency domain). More details related to data processing are reported separately [4]. Briefly, we calculated the PRF from the measured induced voltage (V(t)), using (3)

$$\frac{d}{dH} m(H) = \frac{-1}{\mu_0 \cdot S \cdot \omega \cdot H_0} \cdot \frac{V(t)}{\cos(\omega t)} \tag{3}$$

in which, μ_0 is the magnetic permeability of vacuum ($4\pi \times 10^{-7}$ Vs/Am) and S is the coil sensitivity [1/m]. PRF data obtained from this equation has the unit of [m^3/g Fe] after normalizing by the total amount of the iron in the samples. For harmonic spectra, we used Fourier transform of the MPS signal

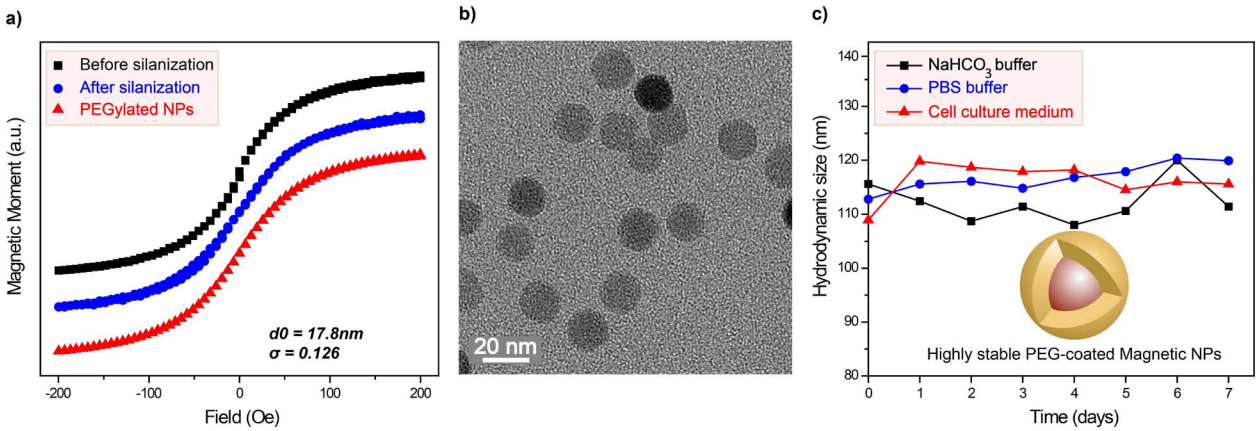

Fig. 1. (a) Normalized m-H curves of the nanoparticles before and after silanization, and after their coating with PEG molecules. The plots are shifted vertically for clarity. The median core size (d_0) and standard deviation (σ) of the PEG-coated NPs were calculated using Chantrell fitting [19]. (b) TEM image of the PEG-coated nanoparticles, showing results in accordance with our m-H size measurements. (c) Stability of the hydrodynamic size of the PEG-coated nanoparticles in different biological solutions as a function of incubation time. Stability plays an important role in long-term MPI performance of the NPs as shown by MPS data presented in Fig. 2.

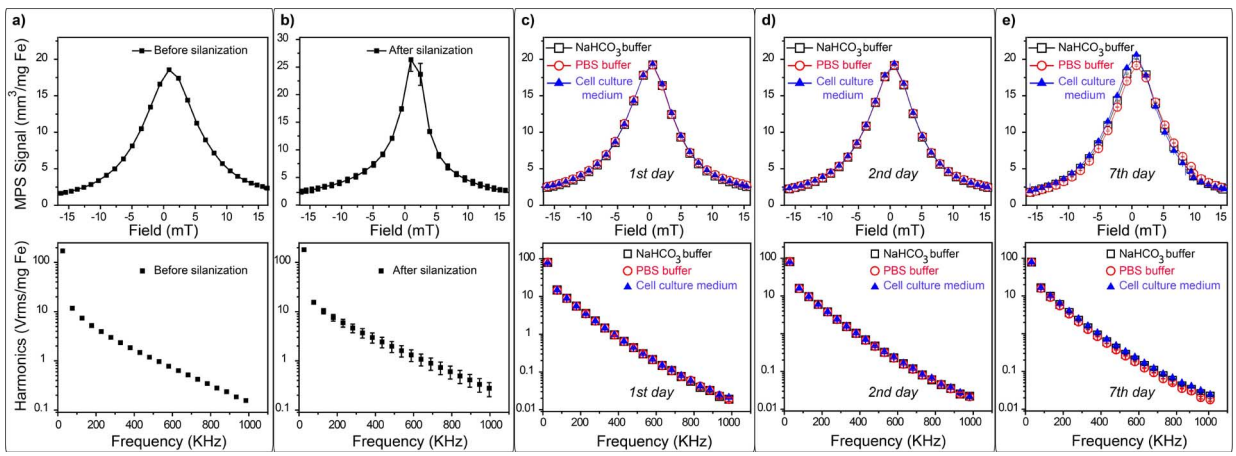

Fig. 2. Particles response function (top) and harmonics (bottom) diagrams of the nanoparticles before (a) and after silanization (b) and PEGylation (c). The PEG-coated NPs showed a consistent signal intensity and spatial resolution after incubation in sodium bicarbonate, PBS and cell culture (DMEM enriched with 10% FBS) media for 2 (d) and 7 days (e).

voltage [9], and the resulting data was normalized by the quantity of the iron in each sample.

III. Results and Discussion

We used a ligand exchange approach to transfer the hydrophobic NPs to aqueous media. NPs were first modified with silane functionalized molecules, which introduces carboxyl groups to the surface of the NPs. DCC was then used to bond bis-amine PEG molecules to these carboxyl groups. Using SPDP assay [20], the average number of active amine groups per NP was estimated to be about 102. As shown in Fig. 1(a), the slope of the m-H curves did not change after coating of the NPs with PEG, showing that the median core size of the NPs did not change considerably during the process. This indicates that no aggregates or cross-linked NPs were formed through the coating reaction and it was confirmed by calculation of the average core sizes of the NPs before and after PEGylation, using the Chantrell fitting [19]. Note that the slight decrease of the magnetization slope after silanization is due to pre-silanization purification process that we used to remove the large aggregates that were formed during the high temperature synthesis of oleic acid coated NPs. The calculated median core size of the PEG coated NPs was 17.8 nm, with a narrow standard deviation of 0.126. These values are 18.35 nm and 0.225 before silanization and 18.06 and 0.04 after silanization. TEM image of the PEG-coated NPs shown in Fig. 1(b), clearly confirms our VSM-based size calculations. The PEG coating cannot be seen in TEM due to its very low contrast in comparison with the crystalline core. Also, it rapidly gets decomposed due to beam damage from the high energy electron beam (i.e., 200 KeV).

PEG-coated NPs had a very narrow hydrodynamic size distribution (Z-average of 112 nm with polydispersity index of 0.189). Due to the electrostatic repulsions between NPs and steric hindrance provided by PEG molecules, NPs were very well stable in biological media, showing an almost constant hydrodynamic size, without formation of aggregates after a week [Fig. 1(c)].

The PRF and harmonic spectra of the NPs at each step of the procedure (Table I) are shown in Fig. 2. Signal intensity (i.e., peak height or harmonic values) and spatial resolution of the NPs were enhanced after silanization [compare Figs. 2(a) and (b)]. Also, the slope of the harmonics spectrum was less

for silanized NPs. As mentioned earlier, these are due to elimination of the larger and smaller fractions of the as-synthesized NPs during the washing process that resulted in narrower size distribution of the NPs after silanization ($\sigma = 0.04$) and is in agreement with the m-H curves [Fig. 1(a)] [4]. This can be also correlated to the increased interaction of the NPs after replacement of the oleic acid with TSP molecules. After coating with PEG, the NPs showed a narrow core and hydrodynamic size distributions. These resulted in their high spatial resolution and signal intensity [Fig. 2(c)]. The PRF peak and 3rd harmonic intensities of the PEG coated NPs were 18.31 ± 0.03 mm^3/mg Fe and 14.91 ± 0.02 V_{rms}/mg Fe, respectively, before starting the incubation. Also, the harmonics spectra of the NPs in different solutions perfectly overlap with each other even up to 39th harmonic. Long-term, the NPs maintained their MPS performance in different biological media, even for up to a week of incubation [Fig. 2(d) and (e)]. We have shown before that there are three possible mechanisms (i.e., Néel, Brownian and hysteretic reversal) for relaxation of the NPs in MPI [4], [7]–[9]. We used (1) and (2) to calculate the Néel and Brownian relaxation times ($\sim$2 and $\sim$300 microseconds, respectively) and compared these values with field switching time in our MPS system ($\sim$40 microseconds) to investigate the relaxation mechanisms of the NPs. The time needed for Brownian relaxation was much higher than field reversal time for the frequency used in our MPS (25 kHz). Therefore, there was no Brownian relaxation contribution in our MPS signals. Also, when hysteretic reversal dominates, the PRF peak occurs at a finite non-zero value that depends on the particle's anisotropy, so that the PRF is asymmetric about the origin [4], [21]. Therefore, symmetrical PRF peak at near zero field range confirms that Neel relaxation was the dominant mechanism, resulting in the consistent MPS performance of the PEG-coated NPs [4].

IV. Conclusion

The nanoparticles reported in this paper show consistent performance, without any agglomeration, suitable for practical MPI measurements related to future cardiovascular imaging, cancer diagnosis and stem cell tracking. In fact, size stability of these NPs in biological media is the crucial parameter required for these applications. It also helps to improve the blood half-life and efficient uptake by the targeted cells or tissues. Furthermore, the presence of amine groups on the surface of the NPs provides abundant chemically active sites for conjugation of other therapeutic or biomolecules. High spatial resolution and signal intensity of these NPs, with the majority contribution from Néel relaxation, makes them promising candidates for a wide range of *in vitro* and *in vivo* MPI applications in the future.

Acknowledgment

This work was supported by NIH Grants 1RO1EB013689-01/NIBIB. Part of this work was conducted at the University of Washington NanoTech User Facility, a member of the NSF National Nanotechnology Infrastructure Network (NNIN). The authors would like to thank H. L. Kaufman for her invaluable laboratory assistance, as well as Dr. R.M. Ferguson and A. Khandhar for helpful discussions.

References

[1] B. Gleich and J. Weizenecker, "Tomographic imaging using the nonlinear response of magnetic particles," *Nature*, vol. 435, pp. 1214–1217, 2005.

[2] K. M. Krishnan, "Biomedical nanomagnetics: A spin through possibilities in imaging, diagnostics, and therapy," *IEEE Trans. Magn.*, vol. 46, no. 7, pp. 2523–2558, Jul. 2010.

[3] P. W. Goodwill, E. U. Saritas, L. R. Croft, T. N. Kim, K. M. Krishnan, D. V. Schaffer, and S. M. Conolly, "X-space MPI: Magnetic nanoparticles for safe medical imaging," *Adv. Mater.*, vol. 24, pp. 3870–3877, 2012.

[4] H. Arami, R. M. Ferguson, A. P. Khandhar, and K. M. Krishnan, "Size-dependent ferrohydrodynamic relaxometry of magnetic particle imaging tracers in different environments," *Med. Phys.*, In Press.

[5] P. W. Goodwill and S. M. Conolly, "The X-space formulation of the magnetic particle imaging process: 1-D signal, resolution, bandwidth, SNR, SAR, and magnetostimulation," *IEEE Trans. Med. Imag.*, vol. 29, no. 11, pp. 1851–1859, Nov. 2010.

[6] J. Rahmer, J. Weizenecker, B. Gleich, and J. Borgert, "Signal encoding in magnetic particle imaging: Properties of the system function," *BMC Med. Imag.*, vol. 9, pp. 1–21, 2009.

[7] R. M. Ferguson, K. R. Minard, and K. M. Krishnan, "Optimization of nanoparticle core size for magnetic particle imaging," *J. Magn. Magn. Mater.*, vol. 321, pp. 1548–1551, May 2009.

[8] R. M. Ferguson, K. R. Minard, A. P. Khandhar, and K. M. Krishnan, "Optimizing magnetite nanoparticles for mass sensitivity in magnetic particle imaging," *Med. Phys.*, vol. 38, pp. 1619–1626, Mar. 2011.

[9] R. M. Ferguson, A. P. Khandhar, and K. M. Krishnan, "Tracer design for magnetic particle imaging," *J. Appl. Phys.*, vol. 111, p. 07B318, 2012.

[10] H. Arami, Z. Stephen, O. Veiseh, and M. Zhang, "Chitosan-coated iron oxide nanoparticles for molecular imaging and drug delivery," *Adv. Polym. Sci.*, vol. 243, pp. 163–184, 2011.

[11] E. C. Stoner and E. P. Wohlfarth, "A mechanism of magnetic hysteresis in hetrogeneous alloys (reprinted from philosophical transaction royal society-London, vol 240, pg 599–642, 1948)," *IEEE Trans. Magn.*, vol. 27, no. 7, pp. 3475–3518, Jul. 1991.

[12] A. P. Khandhar, R. M. Ferguson, and K. M. Krishnan, "Monodispersed magnetite nanoparticles optimized for magnetic fluid hyperthermia: Implications in biological systems," *J. Appl. Phys.*, vol. 109, Apr. 2011.

[13] C. Fang, N. Bhattarai, C. Sun, and M. Q. Zhang, "Functionalized nanoparticles with long-term stability in biological media," *Small*, vol. 5, pp. 1637–1641, July 2009.

[14] A. P. Khandhar, R. M. Ferguson, J. A. Simon, and K. M. Krishnan, "Enhancing cancer therapeutics using size-optimized magnetic fluid hyperthermia," *J. Appl. Phys.*, vol. 111, p. 07B306, 2012.

[15] M. Q. Zhu, E. Chang, J. T. Sun, and R. A. Drezek, "Surface modification and functionalization of semiconductor quantum dots through reactive coating of silanes in toluene," *J. Mater. Chem.*, vol. 17, pp. 800–805, 2007.

[16] A. P. Khandhar, R. M. Ferguson, J. A. Simon, and K. M. Krishnan, "Tailored magnetic nanoparticles for optimizing magnetic fluid hyperthermia," *J. Biomed. Mater. Res. A*, vol. 100, pp. 728–737, Mar. 2012.

[17] S. Kalele, R. Narain, and K. M. Krishnan, "Probing temperature-sensitive behavior of pNIPAAm-coated iron oxide nanoparticles using frequency-dependent magnetic measurements," *J. Magn. Magn. Mater.*, vol. 321, pp. 1377–1380, May 2009.

[18] R. Narain, M. Gonzales, A. S. Hoffman, P. S. Stayton, and K. M. Krishnan, "Synthesis of monodisperse biotinylated p(NIPAAm)-coated iron oxide magnetic nanoparticles and their bioconjugation to streptavidin," *Langmuir*, vol. 23, pp. 6299–6304, May 2007.

[19] R. Chantrell, J. Popplewell, and S. Charles, "Measurements of particle size distribution parameters in ferrofluids," *IEEE Trans. Magn.*, vol. MAG–14, no. 5, pp. 975–977, Sep. 1978.

[20] M. K. Yu, J. Park, Y. Y. Jeong, W. K. Moon, and S. Jon, "Integrin-targeting thermally cross-linked superparamagnetic iron oxide nanoparticles for combined cancer imaging and drug delivery," *Nanotechnology*, vol. 21, Oct. 2010.

[21] J. Weizenecker, B. Gleich, J. Rahmer, and J. Borgert, "Micro-magnetic simulation study on the magnetic particle imaging performance of anisotropic mono-domain particles," *Phys. Med. Biol.*, vol. 57, pp. 7317–7327, Nov. 2012.